Cloud and Aerosol Lidar Technology Systems Study
Final Report

John H. Stadler
NASA Langley Research Center
Hampton, VA 23681
Phone: 757-864-7076; Fax: 757-864-7202
e-mail: j.h.stadler@larc.nasa.gov

Introduction

The composition of the global atmosphere has changed during this century because of human activities. Climate models now predict a significant global warming in response to the rising concentrations of carbon dioxide and other greenhouse gases in the atmosphere. However, confidence in these predictions is low because of significant uncertainties in the modeled radiative effects of aerosols (small suspended particles) and clouds. While passive sensors have some ability to measure aerosol optical depth over oceans, they have great difficulty making this measurement over land, where the majority of anthropogenic aerosol forcing occurs. Passive sensors also have little ability to measure the vertical distribution of tropospheric aerosols, knowledge of which provides valuable information on boundary layer height and aerosol source strength and transport. Spaceborne lidar is currently the only viable technique for obtaining unambiguous, high-spatial-resolution global information on cloud and aerosol spatial distributions and optical properties. This information will significantly improve our understanding of the Earth's radiation budget and improved the current predictive capabilities to enable policy makers to reach balanced decisions on mitigation strategies.

This study investigated the technology requirements to reduce the mission life cycle costs of a cloud and aerosol lidar and enable a High-Spectral Resolution (HSR) lidar. Typical cloud and aerosol lidars provide incoherent backscatter profiles at one or more wavelengths. Figure 1 depicts a lidar block diagram for a basic backscatter lidar. The first spaceborne atmospheric lidar, the Lidar In-Space Technology Experiment (LITE) which flew on Shuttle in 1994 (Winker et al. 1996), operated at the fundamental and frequency doubled and tripled wavelengths of Nd:YAG (1064, 532, and 355 nm). This experiment was an immense success and demonstrated the value of global lidar measurements of cloud and aerosol spatial distributions to the broader atmospheric science community. Figure 2 is a sample of the LITE science data. However, the limitation of such an approach is that, in order to infer extinction profiles and optical depths of cloud and aerosol layers, assumptions must be made on the extinction-to-backscatter ratio at the transmitted wavelength(s). This limitation can be overcome by employing the high-spectral-resolution (HSR) lidar technique (Piironen and Eloranta, 1993; Alvarez et al., 1993).

The HSR lidar technique takes advantage of the spectral distribution of the return signal to discriminate between molecular and aerosol/cloud lidar return signals. Figure 3 shows the spectral distributions of lidar backscatter for both purely molecular and and purely

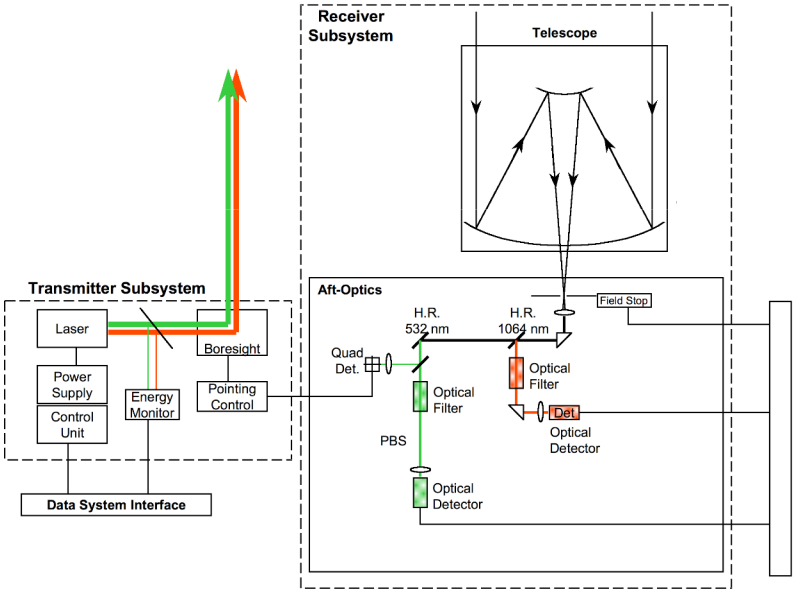

Figure-1 – Simple backscatter lidar functional block diagram

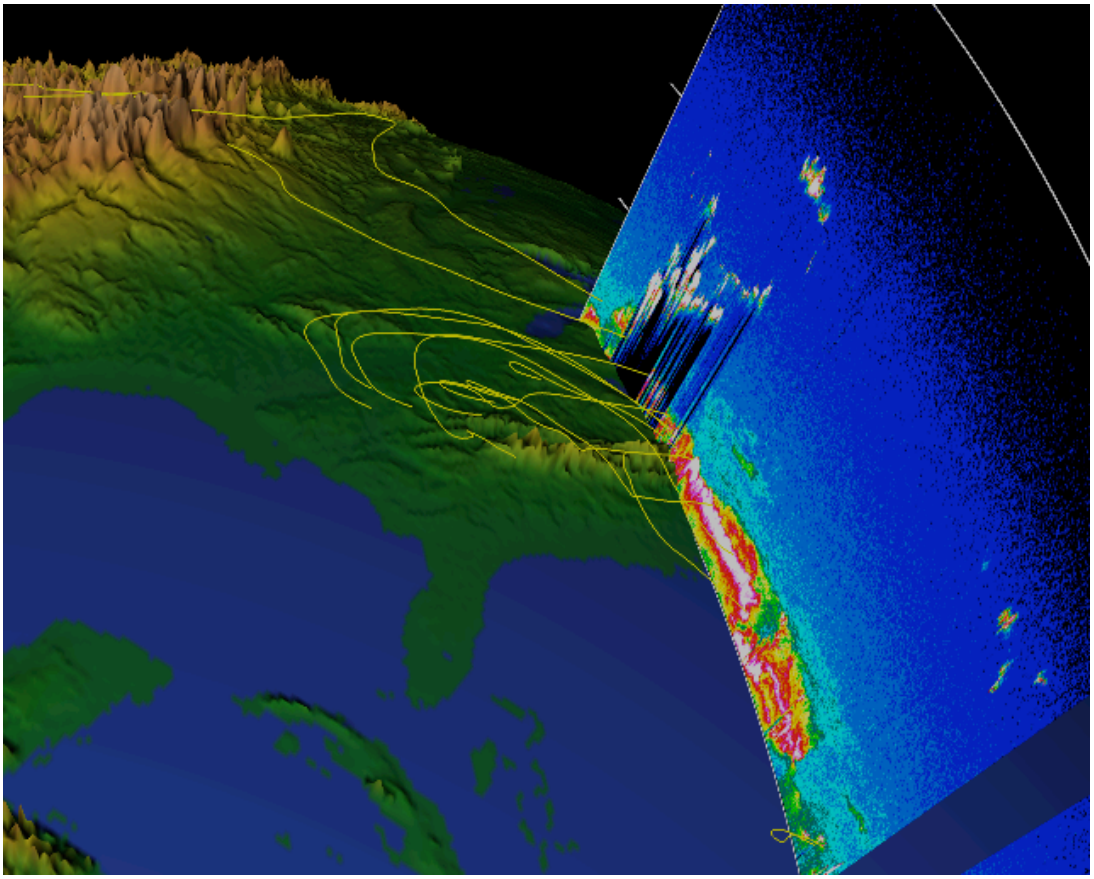

Figure 2. 3-D visualization showing haze (red) over the eastern U.S. observed by LITE. Yellow lines trace air motions over the previous 5 days.

aerosol lidar returns. Lidar backscatter from air molecules is Doppler broadened by approximately 3 GHz due to the high-velocity random thermal motion of molecules. Because the cloud and aerosol particles are much more massive than gas molecules, the Brownian motion of these particles is significantly lower in velocity than the thermal motion of air molecules, and the resulting Doppler broadening of the cloud/aerosol return is negligible. The linewidth of the backscatter from cloud and aerosols, being nearly identical to the laser linewidth (approximately 50 MHz for an injection-seeded laser), is therefore much smaller than that of the Rayleigh return. Unlike standard backscatter lidars, a HSR lidar can discriminate between the frequency-broadened molecular returns and the relatively unbroadened cloud/aerosol returns. The capability to discriminate between signals with such narrow linewidths puts stringent requirements on the linewidth and frequency stability of the laser transmitter and on the frequency resolving capability and stability of the receiver.

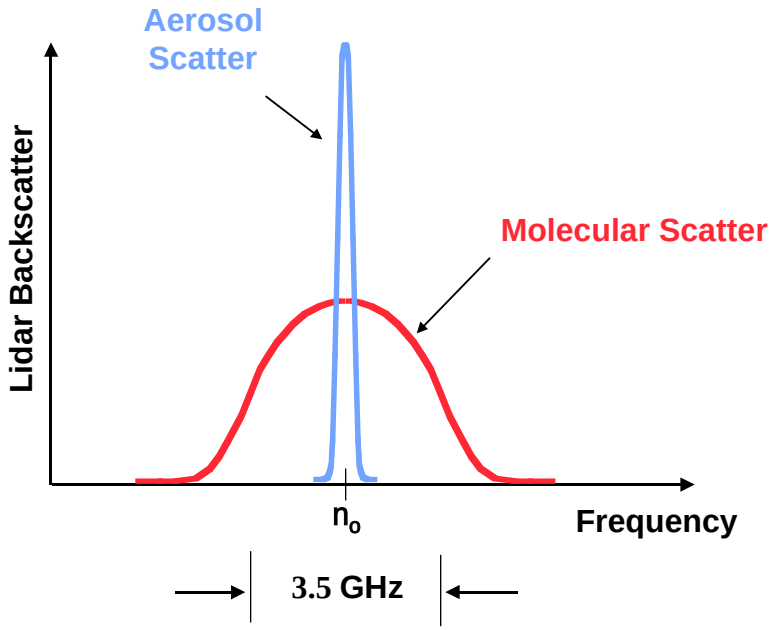

Figure-3. Lidar backscatter spectral distributions for both purely molecular and purely aerosol lidar returns

Study Objective

The objective of this study was to identify key technologies to reduce the mission life cycle costs of spaceborne cloud and aerosol lidar missions, including HSR lidars. Although the title of this study is cloud and aerosol lidars, it is recognized that most atmospheric remote sensing lidars (cloud and aerosol, wind, altimetery, and DIAL) have many common features and technology requirements. Whenever possible, this commonality was considered to enable maximum leveraging of technology development investments.

Methodology

The methodology of this study was to identify cost drivers and then identify technologies that can affect the cost drivers. Several in-house bottoms-up cost estimates have indicted that power is a driving cost factor for lidars. This is not too surprising since lidars are active sensors and typically require significantly more power than passive instruments. For the purposes of this study, the availability of a parametric cost estimate based on power is desired. Unfortunately, there does not exists a parametric cost model based solely on lidars because of the small number of historical samples. Therefore, for this study, cost data was derived from the parametric Small Satellite Cost Model from the Aerospace Corporation (Wertz, J.R. and Larson, W.J., 1996). Since this model is based upon passive Earth sensors it is not totally accurate for active sensors. Therefore, a correction factor, based on bottoms up cost analysis, has been factored into these results. It should be emphasized that this model should be used only for qualitative study.

The next step of the process was to perform parametric trade studies by utilizing the lidar equation (reference Appendix A). The approach was to select a lidar target and required signal-to-noise ratio to meet current scientific objectives. The approach was to maintain a constant signal-to-noise ratio, vary the lidar parameters and determine the required laser power. Laser power will be the only appreciable change to the overall electrical power requirement, since the other lidar electronics, such as instrument controller; signal conditioning; etc, will remain largely unchanged. The following lidar parameters were studied:

Telescope Diameter
Laser Energy, Repetition Rate, and Efficiency
Detector performance (Quantum Efficiency)
Optical Filter Bandwidth and Transmission and laser linewidth

Results

Figure 4 shows the relationship between instrument cost and power based on the Aerospace Corporation's Small Satellite Cost Model modified using a LaRC cost correction factor for active sensors. It should be emphasized that there exists little historical cost data for space based atmospheric lidar systems, therefore this figure should only be used for qualitative analysis.

After examining Figure 4, it becomes apparent that instrument power requirements can have a significant impact on cost. Using the lidar equation presented in Equation 1 we can perform parametric studies on what affects of varying lidar parameters have to instrument power while maintaining a constant science requirement (that is a constant target with a constant signal-to-noise ratio). To ensure proper comparisons, all of the charts are based upon a common measurement objective: Daytime Raleigh return at 1 km with 1 km vertical and 25 km horizontal resolution under daylight conditions. For this target and lighting conditions, a signal-to-noise ratio of at least 13.7 must be maintained to meet current scientific objectives. Other assumed lidar parameters are detailed in Appendix B.

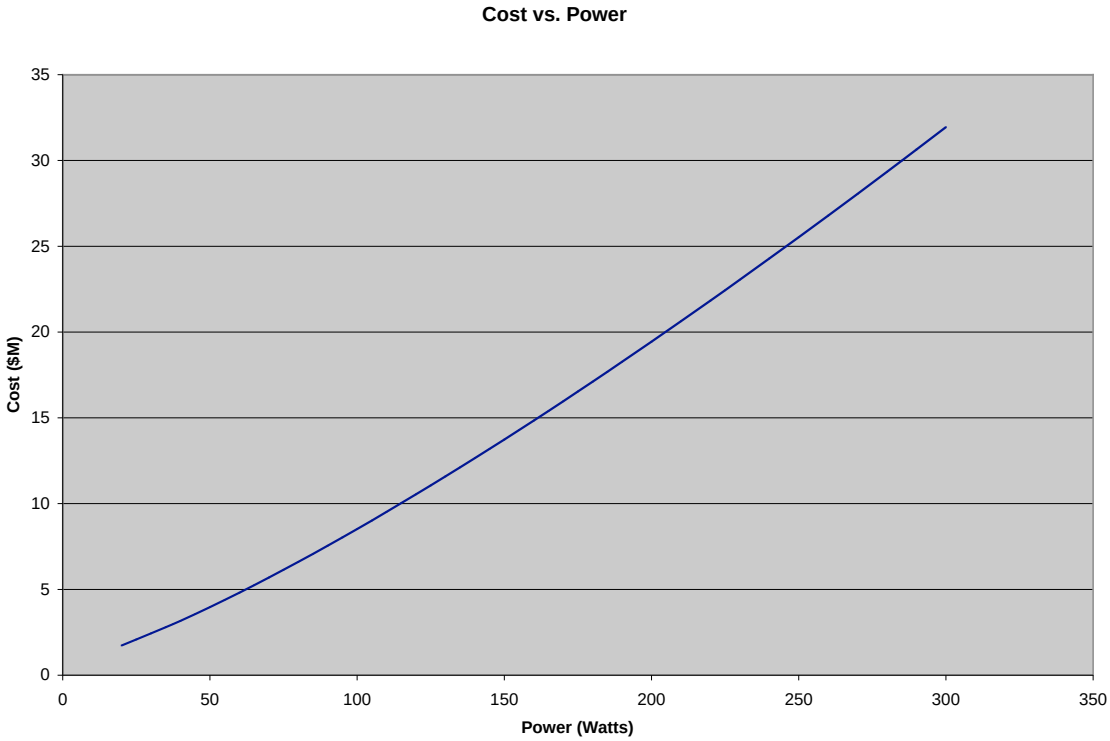

Figure 4 – Cost vs. Power Estimate for Active Remote Sensing Instruments

Equation 1 – Lidar Equation

$$\frac{S}{N} = \left[\frac{\frac{Ks * Energy * AperTrans * OptTransBckSctr}{Range^2}}{\sqrt{\left[\frac{Ks * Energy * AperTrans}{Range^2} + Kb * FOV^2 * OptBW \right] * OptTransBckGrnd}} \right] * \frac{\sqrt{Area * QuantEff * ShotsPerSec * HorizRs * VertRs}}{ExcessNoiseFactor}$$

Where:

$$Ks = \frac{BksctCoeff * AtmTrans2Way * Wavelength}{SpeedofLight * PlamcksConst * OrbitalSpeed}$$

$$Kb = \frac{SolarIrradiance * BGLightFactor * Albedo * Wavelength}{2 * PlancksConst * SpeedofLight^2 * OrbitalSpeed}$$

Studying the lidar equation, it is interesting to note that for daytime conditions (BGLightFactor = 0) the signal-to-noise ratio is not a function of laser power, but laser energy times the square root of the laser pulse repetition rate. Figure 5 shows this effect graphically. The laser power (energy*pulse repetition rate) is a constant, but a higher signal-to-noise ratio is achieved at lower rep rates and higher pulse energy. Of course nothing comes for free, laser lifetime is reduced at higher energy pulse levels and eye-safety levels may be reduced beyond acceptable levels.

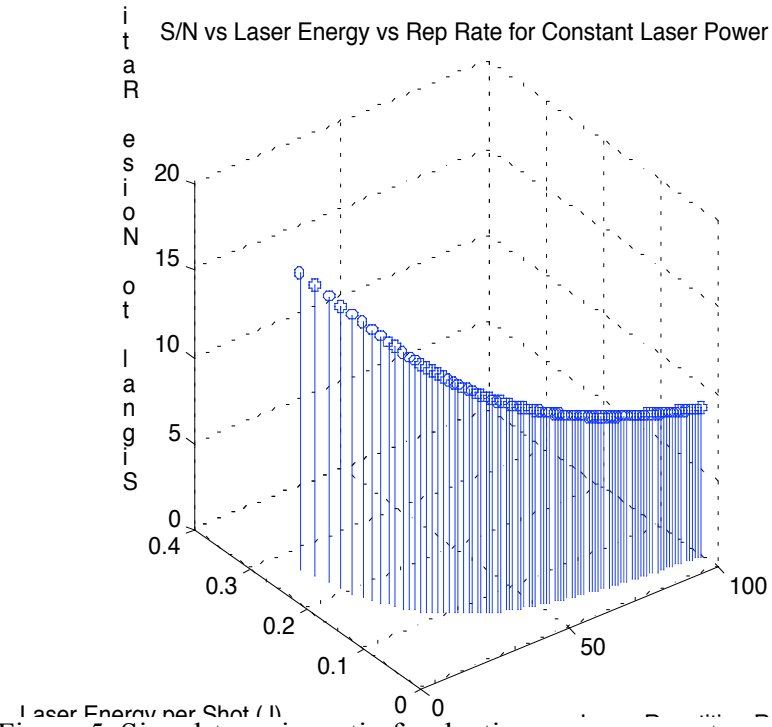

Figure 5. Signal-to-noise ratio for daytime measurements as a function of laser energy and pulse rate where laser energy times repetition rate equals a constant.

The following five figures show the relationship between required laser power and lidar parameter assuming a constant signal-to-noise ratio. It should be noted that the laser repetition rate is held fixed at 27 Hz and only the laser energy is varied. Additionally, these measurements are taken for 532nm wavelength, therefore a 1064 to 532nm conversion rate (optical doubler conversion) is assumed to be a conservative 50% and the wall plug electrical input power to 1064 nm light efficiency is assumed to be 5%.

Figure 6 shows the relationship between required laser power and telescope diameter for a constant signal to noise ratio. It is obvious that increasing the telescope diameter will decrease the required laser power. But there are some practical limits for monolithic telescopes that must be observed. These are the launch vehicle shroud volume, telescope mass, and telescope cost. For space-based applications, a 1-meter diameter telescope is the practical limit. Diameters beyond 1-meter will require lightweight precision deployable telescopes. Figure 6 clearly indicates that a 2.5-meter class telescope is

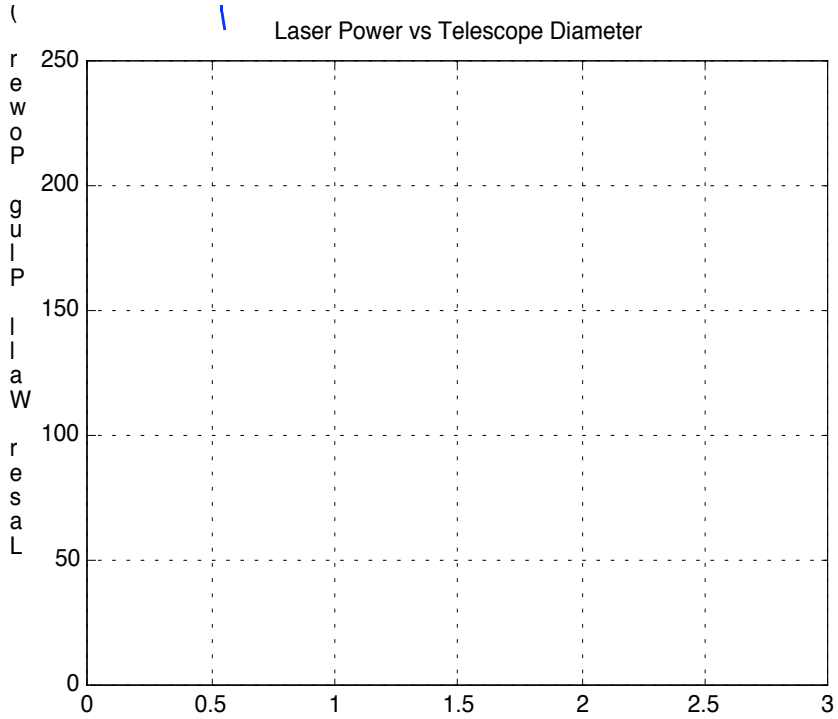

Figure 6. Required laser power vs. telescope diameter

desirable. Since a backscatter lidar is an incoherent measurement, its requirements for mirror surface quality is only about one wavelength. Studies performed at NASA Langley Research Center (Lake, M.S., and Peterson, L.D., 1998) indicate that passive precision deployable telescopes are feasible for lidar-based requirements.

Figure 7 shows the affect of telescope FOV, with matched laser divergence, to the laser power requirement. Clearly, the narrower FOV will significantly reduce the required laser power. It should be noted that the smaller the FOV, the more stringent the mechanical alignment requirements are for the lidar receiver. For mechanical alignment purposes, structural and thermal models indicate that 100 microns is the practical limit. It also should be noted that eye-safety, which is a function of laser pulse energy, wavelength, and laser divergence must be considered.

Figure 8 is the laser power required for varying laser wall-plug efficiencies. The current SOA for Nd:YAG 1-micron lasers is 5-7%. The figure indicates that is desirable to achieve a wall plug efficiency of 10%. For this application, any efficiency above this, yield increasing smaller returns. Currently, Acculight, under a NASA Langley Research Center Contract (NAS1-97118), is building a lab based 10% efficiency Nd:YLF laser. Additionally, Fibertek, Inc., as part of this study, has made recommendations on building a spaced based 10% efficiency 1-micron laser. The Fibertek report can be found in Appendix D.

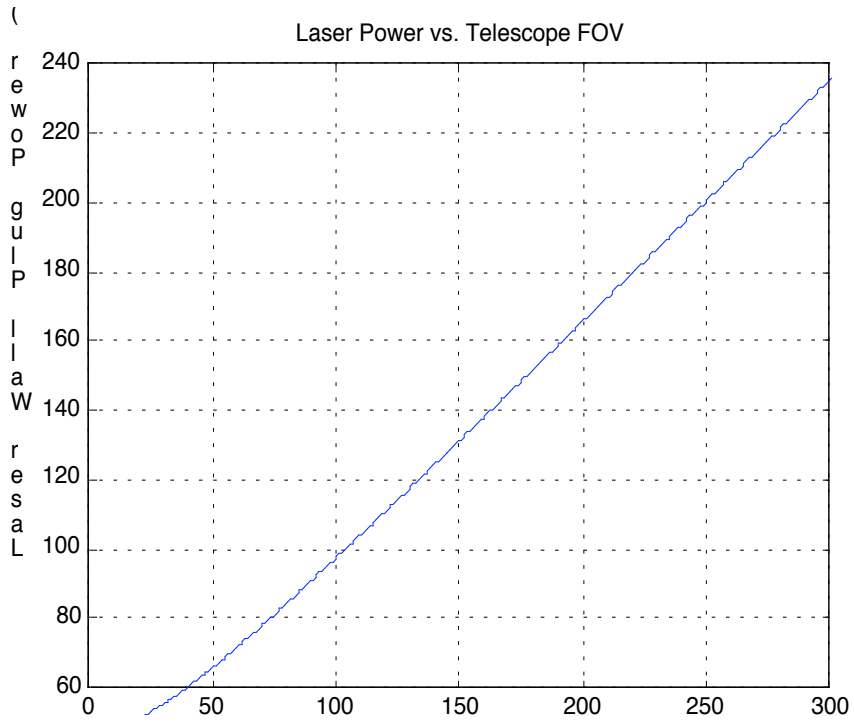

Figure 7. Required laser power vs. telescope FOV assuming matched laser divergene

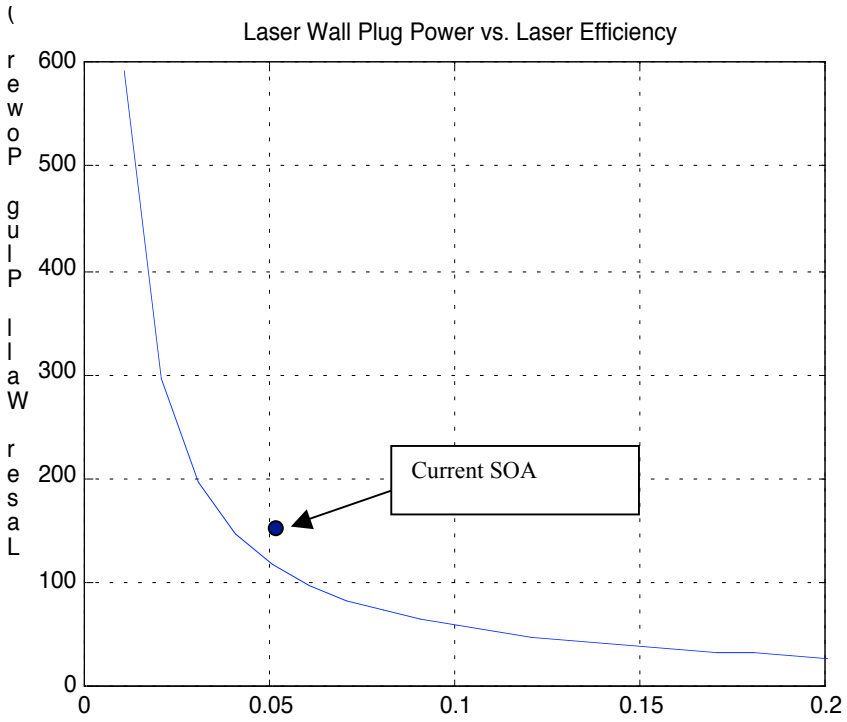

Figure 8. Laser power required for varying laser wall-plug efficiencies

Figure 9 depicts the laser power requirements versus the detector quantum efficiency. It is clear that high quantum efficiency, high gain, low noise detectors with large dynamic range can have a significant impact on power, and therefore, cost requirements.

Figure 10 depicts the power requirement for varying orbital altitudes, or lidar range. Studying Figure 10 and Equation 1 reveals that the S/N ratio is a function of inverse range squared. Therefore the orbital altitude should be carefully chosen. The minimum altitude is going to be a function of atmospheric drag (which is a function of the solar cycle activity), ballistic coefficient, orbital re-boost requirements, and other mission level requirements.

Laser linewidth versus Optical Filter. Appendix C details the calculations involved in evaluating the amount of backscattered energy which is pass through the optical filter. For this design case, the optical filter consists of three optic components. A blocking neutral density filter, and two stacked etalons. The band pass of the blocking filter is 10 times the pass-band of the etalons. The two etalons have the same width but different free spectral ranges. Figure 11 depicts the spectral range of the filter elements. It is clear that more research into the optical filter acceptance angle, pass-band, and transmission efficiency along with the corresponding laser center frequency and linewidth effect the system. It appears that significant gains can be achieved by performing additional research into the controllability of the laser center frequency and linewidth to that of the optical filter center frequency and pass-band. Paramount to this study would be the understanding of the real, as opposed to ideal, laser linewidth and filter pass-band characteristics. It was the intention of this study to further measure and pursue this research. Fibertek was contracted to make linewidth measurements of a diode-pumped space-like laser system. Fibertek's report can be found in Appendix D. Analytical studies were conducted and are presented in Appendix C. Unfortunately, there was not enough time remaining to fully address this issue.

Other Considerations

COTS. To minimize cost, it is advantageous to use a commercial off-the-shelf (COTS) spacecraft bus, such as those offered from the Rapid Spacecraft Development IDIQ, and a small expendable launch vehicle. Based on these constraints, the practical maximum instrument average power is about 300 Watts. With current technology, instrument power much greater than this will force an increase in spacecraft bus size and the need for a larger and significantly costlier launch vehicles.

Eye Safety. Another limitation on the design of a lidar that operates in the visible portion of the spectrum is eye safety. The permissible exposure is a function of the laser frequency, laser energy, laser divergence, and range. These parameters must be carefully balance with the other lidar parameters to maximize S/N ratio while ensuring eye safe operation.

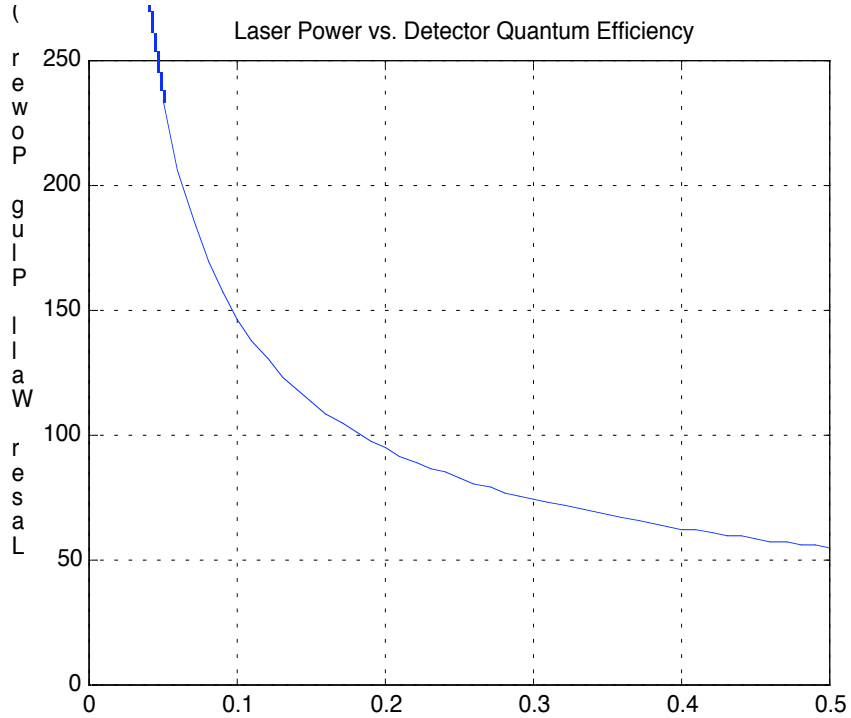

Figure 9. Laser power requirements versus the detector quantum efficiency for a constant target and S/N.

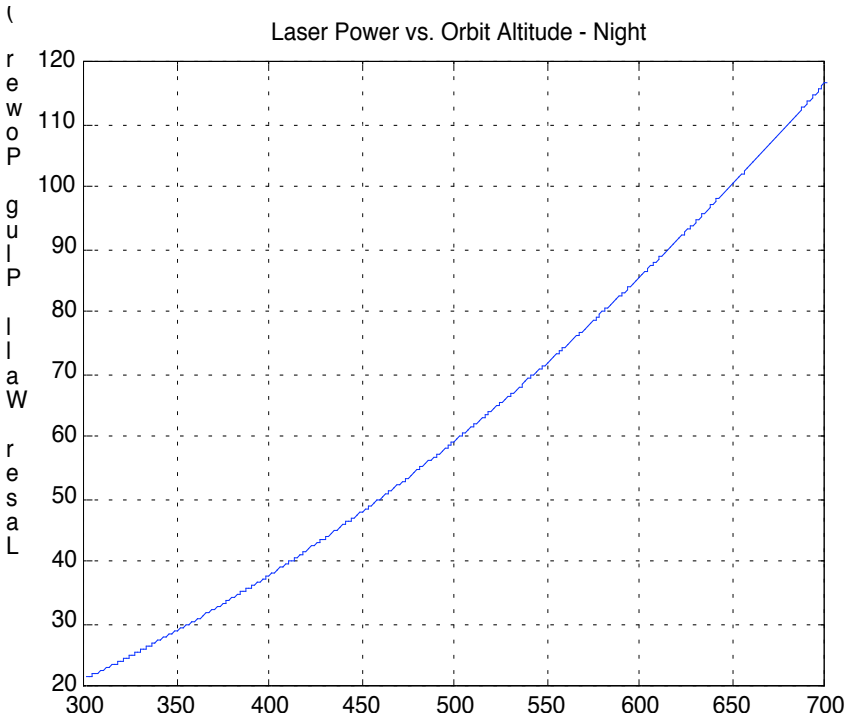

Figure 10. Laser power requirements versus orbit altitude assuming a constant target and S/N.

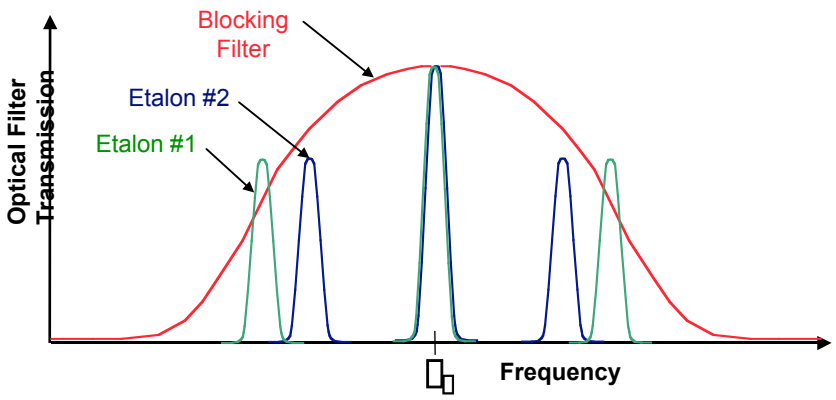

Figure 11. Lidar Receiver optical filter component spectral characteristics.

Recommendations

To reduce the cost and enhance the science return of cloud and aerosol lidar instruments the following recommendation are made with respect to future technology development. Recommendations for High Spectral resolution Lidar Systems are address further below. It is noted when a technology has broader applications beyond cloud and aerosol lidar.

Laser

Current state-of-the-art space based lidar are conductively cooled, diode pumped Nd:YAG lasers operating at approximately 5% wall plug efficiency to 1 micron laser light. The following laser characteristics are desirable for a space-based cloud and aerosol lidar:

- Wavelength: 1.02 to 1.09 μm acceptable, however atmospheric absorption features are to be avoided at both fundamental and second harmonic
- Energy/pulse: >0.2 J at the fundamental and >0.2 J at the second harmonic
- PRF: 10 to 30 Hz
- Pulse length: <50 nsec
- Beam quality: <1.5 times diffraction limit where beam quality is defined as the measured beam divergence over the ideal divergence. For Gaussian beams, this is $\theta_o \omega_f / f\lambda$ where ω_o and ω_f are the beam radii in the near and far field respectively, f is the focal length of the lens used to produce the far field, and λ is the wavelength.
- Beam profile: Smoothly varying in both radial and azimuthal or orthogonal coordinates
- Linewidth: Goal is less than or equal to 5.0 pm at the second harmonic; that is >0.99 of the energy is to be contained in a spectral bandwidth of 5.0 pm or less
- Polarization: >0.99 linearly polarized, fundamental
- Pointing stability: +/- 5% of full-angle laser beam divergence
- Wall Plug efficiency of at least 10%

Detectors

The following detector technologies are recommended:

- Development of APDs with low dark current, low multiplication noise, high multiplication gain, and high quantum efficiency
- Development of PMTs with greater quantum efficiency at 532 nm and 1064 nm
- Detectors and electronics capable of simultaneous photon counting and analog detection (i.e. photon counting through that part of the lidar return exhibiting low signal and analog detection through that part exhibiting high signal).
- Development of methods and materials for extending lifetimes of PMTs
- Development of high speed (> 1GHz) photon counting components including detectors, discriminators, and accumulators
- Development of logarithmic amplifiers which meet the 50 nsec temporal resolution requirement and achieve 7 orders of logarithmic linearity
- Low volume and power consumption.

Telescopes

To enhance lidar capability and reduce costs, development of large aperture, low aeral density deployable telescopes need to be pursued. Recent research at NASA Langley Research Center has indicated that it is possible to build deployable structures that exhibit dimensional stabilities better than one part per *million* - approaching an acceptable level for optical science instruments. Figure 12 depicts a deployable telescope designed by NASA LaRC and Composite Optics Inc. In addition, detailed studies of the "microdynamic" (i.e., sub-micron dynamic) response of these precision structures is leading to a better understanding of how to compensate actively for microdynamic dimensional instabilities that exceed optical metering tolerances. Furthermore, the mirror design can be readily modified to accommodate imaging-quality reflector panels and active panel-alignment control mechanisms for application to imaging telescopes such as NASA's Next Generation Space Telescope, the planned replacement for the Hubble Space Telescope.

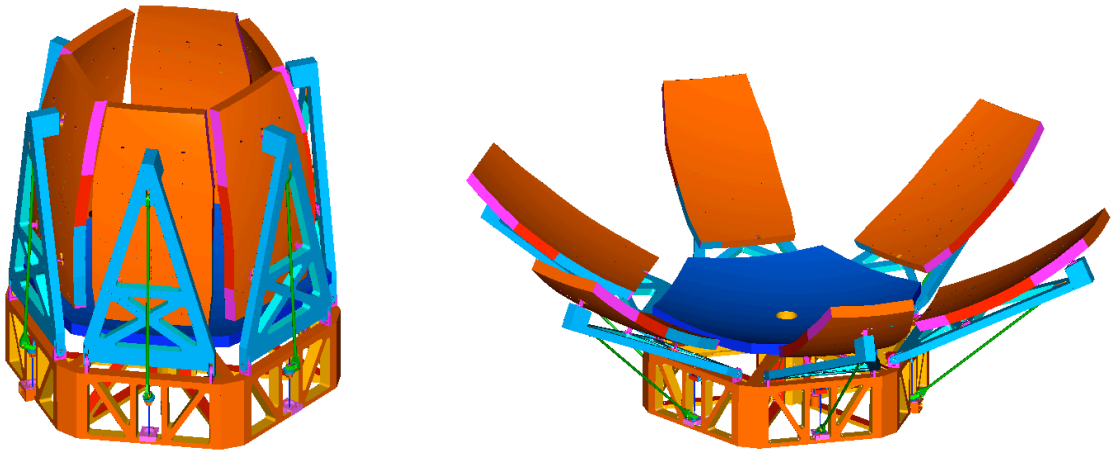

Figure 12. Deployable lidar telescope design developed by NASA LaRC and Composite Optics Inc.

For cloud and aerosol lidar applications, a deployable telescope with an effective diameter of 2.5 meters is highly advantageous. This type and size of telescope is also an enabling technology for some DIAL and Direct Detection Winds Lidars.

Optical Filter

The following optical filter technologies are recommended:

- Optics and filters should be compatible with a large aperture (1-2 m) telescope and a field of view in the range of 100 μradians to 1 mradian.
- Optical technologies for both polarized and unpolarized signal returns will be considered.
- Narrowband optical filters at 532 and 1064 nm should have bandwidths between 5 and 30 GHz and throughput greater than 60%. Narrowband filters must be frequency stable or have a mechanism by which to lock the filter passband to the transmitted laser line.

High Spectral Resolution Lidar Technology Requirements

A research and development program focussed on HSR lidar technologies would significantly hasten the development of long-duration HSR lidar science missions. Also, because many of the technologies required for the HSR lidar application are very similar to those required for the non-coherent wind and DIAL techniques, considerable cross-discipline benefit could be derived from the development of these technologies. Some of the key technology developments that would enable the deployment of a long-duration spaceborne HSR lidar are listed below.

- High electrical-to-optical efficiency (>7%), narrow-linewidth (~50 MHz), frequency-stable, mid-visible, solid-state laser transmitters.
- High-resolution, frequency-discriminating optical receiver systems:
  a) Blocking technique
     - High-throughput (>80%), narrow-band (~8 GHz), frequency-stable optical filters for rejection of background light.
     - High-extinction, narrow-band (~100 MHz), frequency-stable blocking filters or high-throughput (>25%), narrow-band (<1 GHz) , frequency-stable optical filters for the separation of aerosol returns from molecular returns.
  b) Frequency discrimination technique
     - High-spectral-resolution diffractive or interferometric receiver for discrimination and separate detection of aerosol and molecular return signals.

References

Alvarez, R. J. II, L. M. Caldwell, P. G. Wolyn, D. A. Krueger, T. B. McKee, and C. Y. She, Profiling temperature, pressure, and aerosol properties using a high spectral resolution lidar employing atomic blocking filters, *J. Atmos. and Oceanic Tech*., V10, 1993, 546-556.

J. W. Hair, L. M. Caldwell, D. A. Krueger, and C.Y. She, High Spectral Resolution Lidar for Measuring Aerosol and Atmospheric State Parameters Using an Iodine Vapor filter at 532 nm, Application of Lidar to Current Atmospheric Topics, Sedlacek Ed., *SPIE Proceedings 2833*, 1996, 241-250.

Lake, M.S., and Peterson, L.D. (1998). "Research on the Problem of High-Precision Deployment for Large-Aperature Space-Base Science Instruments". *Space Technology and Applications International Forum 1998 Part 1*, January 1998

Piironen, P. and E. W. Eloranta, Demonstration of a high-spectral-resolution lidar based on an iodine absorption filter, *Opt. Lett*., V19, 1994, 234-236.

Wertz, J.R. and Larson, W.J., Reducing Space Mission Costs, *Space Technologies Series, Space Technology Library*, 1996.

Winker, D. M., R. H. Couch, and M. P. McCormick, An overview of LITE: NASA's Lidar In-space Technology Experiment, *Proc. IEEE*, V84, 1996, 164-180

Appendix A

Lidar Equation Derivation

Lidar Technical Note #1

What Determines the Signal-To-Noise Ratio of a Lidar ?

12/22/95

Bill Hunt

Wyle Laboratories
(804) 865-0000 x235
NASA LaRC Mail Stop 901
b.h.hunt@larc.nasa.gov

Abstract

A brief introduction to lidar is given, directed toward readers with little or no knowledge of the subject. Equations are given for the Backscatter Signal, Background Signal, and Signal-To-Noise Ratio (SNR) as a function of atmospheric parameters, instrument parameters, and integration time (vertical and horizontal resolution). Simplified approximations are made for day and night operation.

Background

This Lidar Technical Note (LTN) is one of a series based upon work done in support of the SPARCLE studies (under NASA LaRC contract NAS1-19722). SPARCLE is a concept for a cloud and aerosol lidar operating from a free flying satellite at approximately 500 km altitude (See ***Pre-Phase A Study Report for the Spaceborne Aerosols and Cloud Lidar Earthprobe (SPARCLE), March 15, 1995, NASA Langley Research Center***).

Many of the calculations in the LTN series were done using FREESIM, a Visual Basic simulation program developed to assist in the SPARCLE studies.

Lidar Technical Note #0 serves as an introduction to the series. LTN #0 includes:

- A list of all the technical notes in the series, including brief abstracts of each
- Additional information about SPARCLE science requirements, instrument parameters, and predicted performance
- Some information about FREESIM

Introduction

In designing or evaluating the design of a lidar, it is important to understand how various instrument parameters affect the Signal-To-Noise Ratio (SNR), since the SNR represents the fundamental limitation on what measurements can be made by the lidar.

This LTN begins with a basic introduction to lidar, directed toward those who have little knowledge of the subject. It then presents equations for backscatter and background signals and for SNR. Special emphasis is placed on showing how the various instrument parameters affect the SNR

Scope of Discussion

These SNR discussions are limited to noise sources inherent in the detection process. Noise sources downstream of the detector are a more complicated subject depending upon the electronic design, and are not included in these discussions. Thus the SNR calculations presented here represent the best that a lidar can do, given a certain set of system parameters. An actual system will always do worse.

What Does a Spaceborne Lidar Measure?

The basic measurement made by a spaceborne lidar is atmospheric backscatter.

- A single laser shot gives the atmospheric backscatter at a given geographic location as a function of altitude (backscatter profile) .

- Multiple shots give a series of backscatter profiles as a function of geographic location (latitude and longitude), providing a two-dimensional picture of backscatter along the measurement track.

From a measured backscatter profile, other quantities of interest can be computed. Specifically, the amount of non-molecular scattering can be determined as follows:

- From the molecular density profile, determine the amount of molecular (clean air) backscatter that would be expected. The molecular density profiles can be obtained from atmospheric models or from measured pressure-temperature data. (Pressure-temperature measurements are routinely done at regular intervals through balloon launches at weather stations all over the world).

- Normalize the measured backscatter to the molecular backscatter in an altitude region where there should be no aerosols (typically in the 30-40 km region).

- Over the full altitude span of the measurement, take the ratio of the normalized measured backscatter profile to the molecular backscatter profile. The result is a scattering ratio profile.

- At altitudes where there are no aerosols, the scattering ratio will be unity. Any scattering above the expected molecular scattering (i.e. scattering ratio > 1) is attributed to particles in the air other than air molecules (clouds, volcanic aerosols, dust, smoke, etc.). These non-molecular particles are collectively referred to as aerosols, though that might be a misnomer in some cases.

The simple backscatter lidar cannot directly distinguish among various types of non-molecular particles. Measurements at multiple wavelengths and/or multiple polarizations can provide some additional information, but there are still more unknowns than measurements, so the experimenter must use other knowledge and experience to distinguish among various kinds of non-molecular particles.

How Does a Lidar Work?

A lidar transmits a pulse of laser light down through the atmosphere and measures the backscattered light as a function of time, which can be related to the altitude where the scattering occurred.

- The laser pulse duration is typically around 20 nsec, corresponding to a light pulse 6 meters long.

- The backscattered light is collected with a telescope, which directs the collected light onto a detector - typically a Photomultiplier (PMT) or an Avalanche Photodiode (APD).

- The detector produces photoelectrons in response to the photons falling on its cathode. The detector Quantum Efficiency determines what fraction of the incident photons produce photoelectrons.

- The detector amplifies the photoelectron pulses, producing an output pulse containing many electrons for each photoelectron emitted. Additional amplification is typically provided by the electronics downstream of the detector.

- Range (altitude) resolution is provided by measuring the number of photoelectrons produced in each of many very small time bins (corresponding to backscatter from small altitude segments of the atmosphere). Collectively, the signal values in these altitude bins make up the backscatter profile.

How Do We Measure the Signal Level?

Measurement of the signal level in each altitude bin can be done in one of two ways:

Photon Counting:

If individual photoelectron emissions are sufficiently separated in time, each photoelectron produces a discrete output pulse from the detector (even though each output pulse contains many electrons). In that case a Multichannel Scaler (range-binned photon counter) can be used to count the photoelectron pulses from the detector in each time (altitude) bin. A discriminator is used to exclude any pulses that are too small to have originated with a photoelectron.

Photon counting has several potential advantages over analog processing:

- It is relatively insensitive to low level non-random electronic noise, which can cause significant errors in analog processing at low signal levels.
- It is insensitive to small variations in the detector gain, which can be a factor with analog processing if any kind of system calibration is attempted.
- It has the potential of greater dynamic range than typical analog to digital converters (though that potential may not always be realizable).
- It provides somewhat greater SNR, due to the exclusion of low amplitude noise pulses such as might arise in the amplification process.

If the photoelectron emission rate is too high (typically greater than about 50×10^6 photoelectron/sec), then the output pulses overlap, and photon counting cannot be used. Very high electronic bandwidth (>200 MHz) in order to maximize the usable count rate.

Analog Processing:

If the signal level (photoelectron emission rate) is too high for photon counting, analog processing must be used. For analog processsing, the electonic bandwidth is normally limited to approximately one-half the sample rate (i.e. typically to ~5 MHz), thereby smoothing the output pulses. The smoothed output current is converted to a voltage which is measured at very frequent intervals (typically 10 MHz) using a high speed Transient Digitizer. The dynamic range is nominally limited by the number of digitizer bits (usually 12), though the practical limit at low signal levels is the electronic noise floor, since signal averaging allows signals below one digitizer bit to be resolved.

The choice between photon counting and analog processing is usually based upon the signal levels. Analog processing must be used if the signal levels are too high for photon counting. At lower signal levels, either method may be used, with photon counting preferred. The two methods could be used in parallel for cases where part of the profile has signal levels too high for photon counting, and part does not.

Time and Altitude Relationship

The quantity that is directly measured is the backscatter signal as a function of sample number, which is a function of the time after the start of the measurement. The range and the altitude must be derived from that sample number.

The range from the lidar to the scattering volume is related to the time after laser firing as follows:

$$Range(km) = \frac{SpeedOfLight * TimeAfterLaserFiring}{2} = 0.15 * TimeAfterLaserFiring \quad (usec)$$

Where SpeedOfLight = 0.30 km/□sec

The time between the laser firing and the middle of a given backscatter measurement sample is

$$TimeAfterLaserFiring = MeasurementStartDelay + (SampleNumber - 0.5) * SampleInterval$$

For analog processing, the time sample interval is typically 0.1 microseconds, giving 0.015 km altitude bins, with electronic filtering giving a minimum resolution on the order of twice the altitude bin size. For photon counting, the bins are typically on the order of 1 microsecond (0.15 km).

The relationship between the Range and the Backscatter Altitude is given by

$$BackscatterAltitude = SpacecraftAltitude \frac{Range}{\cos(OffNadirAngle)}$$

where SpacecraftAltitude and BackscatterAltitude are both referenced to local mean sea level, OffNadirAngle is the lidar pointing direction with respect to nadir.

Noise Sources

Noise refers to random variations in the measured signals unrelated to the received light intensity, causing a corresponding uncertainty in the values measured. We consider noise from two sources:

Detection Noise

Photoelectron emission and multiplication are random statistical processes, with one-sigma variability that can be calculated from the number of photoelectrons in the sample. This noise, sometimes called shot noise, has contributions from all photoelectron-like sources -- background light, dark current, and the backscatter signal.

Since shot noise is inherent in the signal, the only way to reduce it is to reduce the unwanted background signal. The contribution that originates with the backscatter signal cannot be eliminated, and determines the absolute minimum noise that can be obtained. While the noise due to the backscatter signal cannot be eliminated, the SNR can be increased by making the backscatter signal larger.

Electronic Noise

In addition to the detection noise, there is always some noise added by the amplification and measurement process. This noise may or may not be random in nature, and is only partially predictable.

The electronic noise is at least partially controlled by the system design, and every effort should be made to eliminate it as much as possible. The objective in any lidar design should be to have it be shot-noise limited (i.e. to have the electronic noise be negligible in comparison with the detection noise). Toward that end, it is desirable to have most of the system gain be in the detector, rather than in the downstream electronics.

While it is understood that there will always be added noise from the electronics, for the remainder of this discussion we will consider only the detection noise.

Terminology

We define some terms that will be used in the equations in the sections that follow:

Albedo	Fraction of the incident background illumination that is reflected
AperTrans	Fraction of the backscatter signal passing through the field stop (aperture)
Area	Receiver effective light collecting area
AtmsTrans2Way	The atmospheric transmission from the lidar to the target and back to the lidar.
Background	The number of photoelectrons from background light, integrated over the vertical resolution and the horizontal resolution.
BGLightFactor	The background light falling on the earth, relative to the Solar Irradiance
BksctCoeff	A measure of the fraction of the incident light backscattered by a target, having units of meter^{-1} steradian^{-1}. This is the fundamental quantity measured by a lidar.
BksctSignal	The number of photoelectrons from the backscatter signal from an atmospheric target, integrated over the vertical resolution and the horizontal resolution.
DarkCountRate	Photoelectron-like pulses per second emitted by a detector when it is dark
DarkCounts	The number of dark photoelectron-like pulses generated by the detector, integrated over the vertical resolution and the horizontal resolution.
Divergence	Laser Divergence (full angle)
Energy	Laser pulse energy (per shot)
ExcessNoiseFactor	Excess Noise Factor of the detector
FOV	Receiver Field Of View (full angle)
H	Altitude of the atmospheric target (above sea level)
HorizRes	Horizontal resolution (horizontal integration span)

Kb	Proportionality constant for Background
Kd	Proportionality constant for Dark Current
Ks	Proportionality constant for Signal
LidarAlt	Altitude of the lidar (above sea level)
Noise	The one-sigma uncertainty in a measurement due to the statistical nature of the measurement.
OptBW	Optical bandwidth (with or without Narrow Band filter)
OptTrans	Overall optical transmission of the receiver, including NB Filter if it is in place, but excluding the field stop (see *AperTrans*)
PlancksConstant	Constant in the equation for the energy of a photon: $E = hc/\lambda$ where h = Planck's Constant, c = speed of light, λ = wavelength Its value is 6.625×10^{-34} joule-sec.
QuantEff	Detector quantum efficiency
Range	Range from lidar to target
SignalToNoise	Bksct Signal/Noise.
ShotsPerSec	Laser repetition rate
SolarIrradiance	Energy density in a given spectral bandwidth reaching the earth from the sun. The value at 532 nm wavelength is 1.842×10^{3} watts m^{-2} μm^{-2}
SpeedOfLight	The speed of light in a vacuum, equal to 0.30×10^{6} km/sec
TotalSignal	The total number of photoelectrons acquired in a sample (sum of *Signal* and *Background and DarkCounts)*.
VertRes	Vertical resolution (vertical integration span)
Wavelength	The wavelength of the lidar transmitter (laser)

Signal, Background and Dark Count Calculations

$$BksctSigPE.\text{Sec} = \left[\frac{BksctCoeff * AtmsTrans2Way * Wavelength}{2 * PlancksConstant}\right] * \left[\frac{Energy}{Range^2}\right] * Area * QuantEff * OptTrans * AperTrans$$

The lidar equation for the backscatter signal intensity (rate) can be written as:

The background signal intensity can be written as:

$$BackgrndSigPE.\text{Sec} = \left[\frac{SolarIrradiance * BGLightFactor * Albedo * Wavelength}{4 * PlancksConstant * SpeedOfLight}\right] * FOV^2 * FilterBW * Area * QuantEff * OptTrans$$

The dark signal intensity is ***DarkCountRate***

The mean levels of the background signal and the dark signal must be subtracted from the overall signal in order to obtain the backscatter signal. It is important to note that the noise due to these signals remains, even after the mean levels are subtracted.

For purposes of calculating noise and signal to noise, it is useful to express these signals in terms of integrated photoelectrons over the integration time defined by the horizontal resolution

$$IntegrationTime = \left[\frac{HorizRes * ShotsPerSec}{OrbitalSpeed}\right] * \left[\frac{2 * VertRes}{SpeedOfLight}\right]$$

and the vertical resolution:

where the first term is the number of shots during the time the lidar covers a distance equal to HorizRes (km), and the second term is the sample time (seconds) corresponding to an altitude span equal to VertRes(km).

Multiplying the expressions for the signal intensities by the integration time, we get the following expressions for integrated photoelectrons.

$$BackscatSignal = \left[\frac{BksctCoeff * AtmsTrans2Way * Wavelength}{SpeedOfLight * PlancksConstant * OrbitalSpeed}\right] * \left[\frac{Energy}{Range^2}\right] * Area * QuantEff * OptTrans * AperTrans * ShotsPerSec * HorizRes * VertRes$$

$$= Ks * \left[\frac{Energy * AperTrans}{Range^2}\right] * Area * QuantEff * OptTrans * ShotsPerSec * HorizRes * VertRes$$

$$Background = \left[\frac{SolarIrradiance * BGLightFactor * Albedo * Wavelength}{2 * PlancksConstant * (SpeedOfLight)^2 * OrbitalSpeed}\right] * FOV^2 * OptBW * Area * QuantEff * OptTrans * ShotsPerSec * HorizRes * VertRes$$

$$= Kb * FOV^2 * OptBW * Area * QuantEff * OptTrans * ShotsPerSec * HorizRes * VertRes$$

$$DarkCounts = \left[\frac{2}{OrbitalSpeed * SpeedOfLight}\right] * DarkCountRate * ShotsPerSec * HorizRes * VertRes$$

$$= Kd * DarkCountRate * ShotsPerSec * HorizRes * VertRes$$

where we have grouped non-system parameters into constants Ks, Kb, and Kd.

Signal-To-Noise Ratio Calculations

The one-sigma noise at the detector cathode due to the statistical nature of a light measurement is equal to the square root of the total signal (number of photoelectrons) in the measurement.

The noise at the anode (output) is equal to the noise at the cathode multiplied by an ExcessNoiseFactor to account for the additional noise from the electron multiplication process:

$$Noise = \sqrt{TotalSignal} * ExcessNoiseFactor$$

$$= \sqrt{BksctSignal + Background + DarkCounts} * ExcessNoiseFactor$$

$$= \sqrt{\left[\frac{Ks * Energy * AperTrans}{Range^2} + Kb * FOV^2 * OptBW\right] * Area * QuantEff * OptTrans + Kd * DarkCountRate} * \sqrt{ShotsPerSec * HorizRes * VertRes} * ExcessNoiseFactor$$

NOTE

There are differing definitions of ExcessNoiseFactor. In the above equation, ExcessNoiseFactor is defined through the relationship

$$Noise_{Anode} = Noise_{Cathode} \times ExcessNoiseFactor = \sqrt{TotalSignal} \times ExcessNoiseFactor$$

This is the definition used in FREESIM.

Another commonly used definition puts ExcessNoiseFactor inside the square root, resulting in an ExcessNoiseFactor value that is the square of the value as defined above.

Using values for BksctSignal and Noise from the previous equations:

$$SignalToNoise = \frac{Ks * \left[\frac{Energy * AperTrans}{Range^2}\right] * Area * QuantEff * OptTrans * \sqrt{ShotsPerSec * HorizRes * VertRes}}{\sqrt{\left[\frac{Ks * Energy * AperTrans}{Range^2} + Kb * FOV^2 * OptBW\right] * Area * QuantEff * OptTrans + Kd * DarkCountRate} * ExcessNoiseFactor}$$

Note that the Signal in this expression is the <u>total backscatter signal</u>. If the desired measurement is some other quantity (e.g. the aerosol component of the backscatter), then the SNR equation should include that desired signal, rather than total backscatter.

If we assume that **Dark Count Rate << Backscatter Signal Intensity**, we can simplify the above equation :

$$SignalToNoise \_ \left[\frac{\frac{Ks * Energy * AperTrans}{Range^2}}{\sqrt{\frac{Ks * Energy * AperTrans}{Range^2} + Kb * FOV^2 * OptBW}}\right] * \frac{\sqrt{Area * QuantEff * OptTrans * ShotsPerSec * HorizRes * VertRes}}{ExcessNoiseFactor}$$

We can further simplify the equation for **two limiting cases**:

Dark Night: Background << Backscatter and DarkCountRate << Backscatter

$$SignalToNoise = \frac{\sqrt{Ks * Energy * AperTrans}}{Range} * \frac{\sqrt{Area * QuantEff * OptTrans * ShotsPerSec * HorizRes * VertRes}}{ExcessNoiseFactor}$$

$$SignalToNoise \quad \sqrt{\left[\frac{Energy}{Range^2}\right] * ShotsPerSec}$$

Note that for the dark night case the SNR depends upon the product of Energy and ShotsPerSec, which is the average power. Thus we can decrease the pulse energy with no change in SNR so long as we increase the laser rep rate so as to keep the average power constant.

Bright Day: Backscatter << Background and DarkCountRate << Backscatter

$$SignalToNoise = \frac{Ks * Energy * AperTrans}{FOV * Range^2 * \sqrt{Kb * OptBW}} * \frac{\sqrt{Area * QuantEff * OptTrans * ShotsPerSec * HorizRes * VertRes}}{ExcessNoiseFactor}$$

$$SignalToNoise \quad \left[\frac{Energy}{Range^2}\right] * \left[\frac{1}{FOV}\right] * \sqrt{ShotsPerSec}$$

For the bright day case, the SNR directly proportional to Energy, but is proportional to the square root of ShotsPerSec. Now if we decrease the pulse energy while keeping the product of Energy x ShotsPerSec constant, the Signal-To-Noise Ratio will decrease, unlike the dark night case.

The above discussions assumes that the FOV is not changed when the Energy is changed. However, it can be shown that if the FOV and Divergence are changed appropriately when the Energy is changed, it is possible to maintain the same SNR when constant power is maintained. This is discussed in Lidar Technical Note #2.

Validity of Approximations

As an aid in evaluating the validity of the various approximations, let us look at some SPARCLE signal values (as computed by FREESIM).

Dark Count Rate

BksctSigPE.Sec at 40 km, with filter in = 7.7×10^{4} /sec (weakest signal of interest)
DarkCountRate = 2.5×10^{3} /sec

We see that the approximation Dark Count Rate << Backscatter Signal Intensity is a good one for all SPARCLE signals of interest. However, if a detector with high DarkCountRate were to be used, then the approximation might not be valid for the weaker signals.

Night Background

Filter Out:	BksctSigPE.Sec at 40 km = 1.3×10^{5} (weakest signal of interest)
	BGPE.Sec (Full moon, High Albedo) = 1.0×10^{6}
	BGPE.Sec (Full moon, Low Albedo) = 1.3×10^{5}
	BGPE.Sec (Quarter moon, High Albedo) = 1.0×10^{5}
	BGPE.Sec (Quarter moon, Low Albedo) = 1.3×10^{4}
Filter In:	BksctSigPE.Sec at 40 km = 7.7×10^{4} (weakest signal of interest)
	BGPE.Sec (Full moon, High Albedo) = 7.0×10^{2}

We see that the approximation Background << Backscatter is valid for dark night with the filter out, but not for brighter nights. With the filter in at night, the approximation is valid for all lighting conditions.

Day Background

Filter In:	BksctSigPE.Sec (Subvisible Cirrus) = 1.3×10^{7} (weakest signal of interest)
	BksctSigPE.Sec (Cirrus) = 3.0×10^{8} (moderate signal)
	BGPE.Sec (High Albedo) = 3.1×10^{8}
	BGPE.Sec (Low Albedo) = 3.9×10^{7}

During the day, the approximation Background >> Backscatter is valid for the most difficult measurement conditions (weak signal, high albedo), but is not true for stronger signals and lower albedo

Typical Parameter Values

It is informative to look at the range of parameter values that might go into the equations in this LTN.

Table 1 on the following page gives the SPARCLE parameter values, a column indicating whether a High or Low value for a parameter gives a better SNR, and a column indicating the possible range of parameter values. Where there is no well defined limit, estimates are given of reasonable practical limits. These estimates should not be taken too literally.

Parameter	SPARCLE value	Value for best SNR	Possible range of values; Comments
Energy	300 mj	High	>0; generally < 500 mj at 532 nm
ShotsPerSec	10 /sec	High	>0; typically 10 to 50 /sec (see Power)
Power (Energy x ShotsPerSec)	*3 watts*	*High*	*>0; Power is limited by available spacecraft power; A reasonable upper limit for typical medium sized spacecraft might fall in the 3-10 watt range.*
Area	0.63 m^2	High	>0; Limited only by volume, weight, and cost; ~1.0 m^2 practical upper limit for non-deployable
OptTrans	0.50 (NB filter out) 0.30 (NB filter in)	High	0 to 1.0
OptBW	265 nm (NB filter out) 0.3 nm (NB filter in)	Low	>0; NB filter BW limited by laser line width and filter technology. Difficult to go a lot below 0.3 nm with reasonable optical transmission
FOV	0.30 mrad (night) 0.20 mrad (day)	Low	>0; Lower limit set by laser divergence, which in turn is limited by eye safety considerations. 0.20 mrad is near the lower limit for E=300 mj and Alt=500 km.
AperTrans	0.99 (night) 0.87 (day)	High	0 - 1.0 (a function of FOV/Divergence and misalignment angle)
QuantEff	0.14	High	0 - 1.0 (0.14 typical of PMTs; 0.6 typical of APDs at 532 nm)
DarkCount Rate	2.5 x 10^3 /sec	Low	>0; No fixed upper limit 10^3 /sec typical of uncooled PMTS; APDs typically significantly higher
ExcessNoise Factor	1.225	Low	$ 1.0 1.2 typical of PMTs; APDs typically significantly higher
Range	~500 km to surface	Low	~400 km minimum practical spacecraft altitude for long duration flight
HorizRes	0.7 to 300 km (depends on target)	High	>0; lower limit set by pulse repetition rate; upper limit set by science requirements
VertRes	0.03 to 5 km (depends on target)	High	>0; lower limit set by system sample rate and bandwidth; upper limit set by science requirements

Table 1

Appendix B

Assumed Lidar Parameters Used for This Case Study

The following are the initial performance parameters and constants chosen for this test case:

BksctCoeff = 1.45E-06;
AtmsTrns2Way = 0.63;
Wavelength = 5.32E-07;
SpeedofLight = 3.00E+08;
PlancksConstant = 6.625E-34;
OrbitalSpeed = 6.76;
SolarIrradiance = 1.84E+03;
BGLightFactor = 1;
Albedo = 0.15;

Energy = 0.11;
AperTrans = 0.791;
FOV = 1.30E-04;
Range = 705000;
OptBW = 3.00E-05;
Diameter=1;
Area=pi*Diameter^2/4*0.845;
QuantEff = 0.14;
OptTransBackground = 0.416;
OptTransBackscatter = 0.27;
ShotsperSec = 27;
HorizRes = 25;
VertRes = 1000;
ExcessNoiseFactor = 1.225;

Appendix C

Optical Transmission of Backscatter Light Calculations

This appendix is included as a separate file. The file name is:
CAL_Study_Appenix_C.pdf

Appendix D

Fibertek Laser Line Width Measurements

Final Report
For
Lightweight Laser Linewidth Measurements

Prepared By:

Fibertek, Inc.
510 Herndon Parkway
Herndon, Virginia 20170
(703) 471-7671

Submitted To:

NASA Langley Research Center
Hampton, VA 23681-0001

Contract # NAS5-32359
Task 004

Purpose

A laser performance parameter that is critical to the design of a lidar receiver is the spectral linewidth. Etalon filters will be used in the input to the receivers in order to minimize the solar background reaching the receiver detectors. The original specifications for the laser gave a goal of < 90 pm for the 1064 nm linewidth and a goal of < 45 pm for the 532 nm linewidth. More recent modeling of the system performance has indicated that narrower linewidths than the initial specification might be useful in improving the output signal-to-noise (S/N) (Ref. 1).

Before the delivery of the PICASSO-CENA prototype laser in mid-September 1998, a set of preliminary linewidth measurements was performed on the 532 nm output (see Appendix 1). These measurements found the linewidth to be on the order 35 pm. The results were based on simple transmission measurements of fixed solid etalons and thus required an assumption of a particular lineshape function for the laser output. The uncertainty as to the most appropriate lineshape function resulted in a relatively high uncertainty for the linewidth estimates. The purpose of this study is to more accurately characterize the spectral linewidth of both 532 nm and 1064 nm of a space based lidar laser.

The laser on which we have chosen to perform the linewidth measurements is the Lightweight Laser built by Fibertek for the Army Night Vision & Electronic Sensors Directorate (NVESD). There are two primary reasons for this choice. The first is that the laser is currently in-house at Fibertek and is available for use in the linewidth measurements. The second reason is that the Lightweight Laser optical design was the basis for the PICASSO prototype and consequently the two lasers have nearly identical optical designs. The only difference is that the overall cavity length of the Lightweight Laser is ~ 63 cm, compared to ~ 76 cm for the RRL. Thus, we expect the linewidth of the Lightweight Laser to be very similar to that of the RRL. If there were a measurable effect, we would expect the longer cavity of the RRL to improve its beam quality and narrow its linewidth relative to the linewidth of the Lightweight Laser.

Experimental

The approach we chose to perform the linewidth measurements used a commercially available spectrum analyzer capable of characterizing the spectral composition of either pulsed or cw lasers. The device we chose to procure for this purpose was a Burleigh model 3600 Resolver. The particular instrument we chose for these measurements was configured with a Fizeau etalon whose free spectral range was 250 GHz. The etalon coatings were broadband metal coatings that could be used for the analysis of laser wavelengths between 400 nm and 1100 nm. The finesse of the etalon is specified to be >25 over the full spectral range.

For the initial linewidth measurements, a KTP doubling crystal was reinstalled into the Lightweight Laser. This resulted in the conversion of ~55% of the 1064 nm

fundamental output of the laser to 532 nm. With the laser in this configuration, the linewidth of both the 1064 nm and 532 nm output was measured for total output energies up to 70% of the maximum system output of 390 mJ per pulse at 10 Hz. When the total output energy was increased beyond the 70% level, damage to the KTP crystal resulted. An investigation of the cause of this damage found that the q-switch was no longer optimally aligned for hold-off and prelase of the laser had caused the damage. The q-switch and hold-off waveplates were realigned to give hold off up to the full output level of the laser. Unfortunately, there were no spare KTP crystals and no further measurements of the 532 nm linewidths were possible.

Although it was not possible to perform the 532 nm measurements beyond the 70% output energy level, measurements of the 1064 nm linewidth were performed over the full range of output energies by simply removing the damaged KTP crystal. The pure 1064 nm measurements were also performed at 10 Hz. The experimental set-up for both the initial 532 nm plus 1064 nm measurements as well as the 1064 nm only measurements is shown in Figure 1. An uncoated wedge split off ~4% of the beam to be analyzed. This 4% was then directed into the spectrum analyzer with a final folding mirror. A 50 shot average spectrum was recorded for each test condition and then subsequently analyzed to determine the full width at half maximum (FWHM) of the spectral output.

In order to establish the resolution of the system at 1064 nm, the linewidth of a cw diode pumped laser was measured with essentially the same set-up shown in Figure 1. The specified linewidth for the cw laser of <2 GHz was well under the expected resolution of 10 Ghz for an etalon with a free spectral range of 250 GHz and a finesse of 25. This is the minimum value specified by Burleigh for the full 400 nm – 1100 nm operational range. Thus, a measurement of the apparent linewidth of the cw laser provides a good estimate of the actual spectrum analyzer resolution.

Results of System Resolution Measurements

A 50 shot average spectrum was obtained for the relatively narrow line low power cw 1064 nm source. For smooth spectra such as the one, we found that the built in FWHM function of the pulsed spectrum analyzer worked well. The value of the FWHM obtained this way was 3.81 GHz. This is implies that the actual finesse of the etalon at 1064 nm is 66, significantly higher the minimum specification of 25 given by Burleigh. A comparable narrow cw source was not available at 532 nm, so a measurement of the system resolution at 532 nm was not possible.

Results for Simultaneous 532 nm and 1064 nm Operation

The first set of data taken was the measurement of the lineshape and width of the output of the Lightweight Laser with the KTP doubler in place to generate simultaneous 532nm and 1064 nm output. This is the same operational mode as the RRL.

Initially, we attempted to use the built-in FWHM measurement function of the spectrum analyzer to measure the linewidths. This built-in function can be used in a variety of ways. It can be used in real time to show the FWHM of a waveform that is being continuously updated (either single-shot or averaged) or it can be applied to a waveform that is in the spectrum analyzer's buffer memory after active data acquisition has been paused. In addition, it can be used in a record mode to generate a file containing multiple sequential measurements of the FWHM of a series of single-shot waveforms. We did not find the internal FWHM function gave consistent results for any of these modes of operation. At this time, we believe the difficulty is the highly modulated nature of the spectra resulting from the q-switched laser output. Due to this modulation, the software associated with the FHWM function did not always properly identify the true peak of the spectrum. In addition, modulation near where the full width was being measured resulted in shot-to-shot inconsistencies reported by the internal measurement function. In an attempt to smooth the data for better analysis, we tried both Lorenztian and Gaussian fits of the data before measuring the FWHM. Neither of these waveforms provided adequate fits of the data for proper measurements of the FWHM, especially in the case of the 1064 nm waveforms.

The approach we used to measure the FWHM was to simply record 50 shot averaged spectra, plot them out individually, and manually measure the FWHM on the plots. The spectra used for these measurements are shown in Figure 2. For convenient comparison and analysis, all spectra were normalized to have a peak intensity of 100. The results of these FWHM measurements are summarized in Table 1. Two different total output energies were used for the measurements, 130 mJ (70 mJ of 532 nm plus 60 mJ of 1064 nm) and 245 mJ (135 mJ of 532 nm plus 110 mJ of 1064 nm). The 245 mJ total energy operational mode is very similar to that of the RRL except that the repetition rate is reduced to 10 Hz compared to 27 Hz for the RRL.

Table 1. Measured linewidths for simultaneous 532 nm and 1064 nm operation.

Total energy (mJ)	532 nm energy (mJ)	1064 nm energy (mJ)	532 nm FWHM (pm)	1064 nm FWHM (pm)
130	70	60	22	28
245	145	110	14	17

Results for Simultaneous 1064 nm Only Operation

The 1064 nm FWHM measurements were performed in the same manner as for the 532 nm measurements. Figure 3 shows the 50 shot average spectra on which the analyses were performed. For convenient comparison and analysis, all spectra were normalized to have a peak intensity of 100. An unexpected feature of the 1064 nm results was the significant narrowing of the spectra at increased output energies. This is due to the formation of a central spike whose amplitude increases with increasing output energy. This was an unexpected result, but the phenomenon was repeatable for various input beam alignments and intensity and appears to be real. The results of the FWHM measurements are summarized in Table 2.

Table 2. Measured linewidths for pure 1064 nm operation.

Pulse energy (mJ)	40	90	130	200	250	290	340	390
FWHM	10.8	9.5	7.2	4.4	4.6	4.5	5.2	4.4
FWHM	41	36	27	17	17	17	20	17

Conclusions

The results of the FWHM measurements reported here show that for all of the output energies measured, the Lightweight Laser would easily meet the original linewidth requirements for the PICASSO mission, < 45 pm for 532 nm and < 90 pm for 1064 nm. As discussed earlier, we expect the RRL linewidth to be comparable to or slightly less than that of the Lightweight Laser. Based on the results shown in Tables 1 and 2, we would conclude that the linewidth requirements for PICASSO could in fact be significantly narrowed and still be met with the current RRL design, even at significantly higher pulse energies.

A surprising result of these measurements was the observed spectral narrowing of the 1064 nm output with increasing output energy. This was due to the increasing contribution of a narrow central peak with increasing pulse energy. The fact that this structure was consistent for a variety of inputs to the spectrum analyzer and that it did not appear in the low power cw measurements supports our conclusion that the structure is not an experimental artifact. The lack of a similar feature in the 532 nm output is puzzling. Further studies to validate the observed 1064 nm structure would be advised.

The structure of the 1064 nm output has system ramifications for using FWHM data for estimating etalon transmissions. As the spike feature becomes more dominant, the total energy contained within the FWHM of the output can actually decrease. A more detailed analysis of the energy content of the laser output as a function of bandwidth is another area of investigation we would recommend.

An interesting final area of comparison in the reported data is the linewidth of the 1064 nm output with and without second harmonic generation. It might be argued

that the doubling process could affect the distribution of the residual 1064 nm output. The results in Tables 1 and 2 do not show such an effect. For a total energy output energy of 130 mJ, the linewidth is 28 pm with doubling and 27 pm without. A comparison of 245 mJ output with doubling to 250 mJ without doubling finds the same FWHM of 17 nm. Clearly, second harmonic generation is not having a measurable effect on the residual 1064 nm output of the Lightweight Laser, and by analogy is not expected to have an effect on the RRL 1064 nm output.

References

1. Bill Hunt, NASA LaRC, private communication.

Figure 1. Experimental set-up for linewidth measurements.

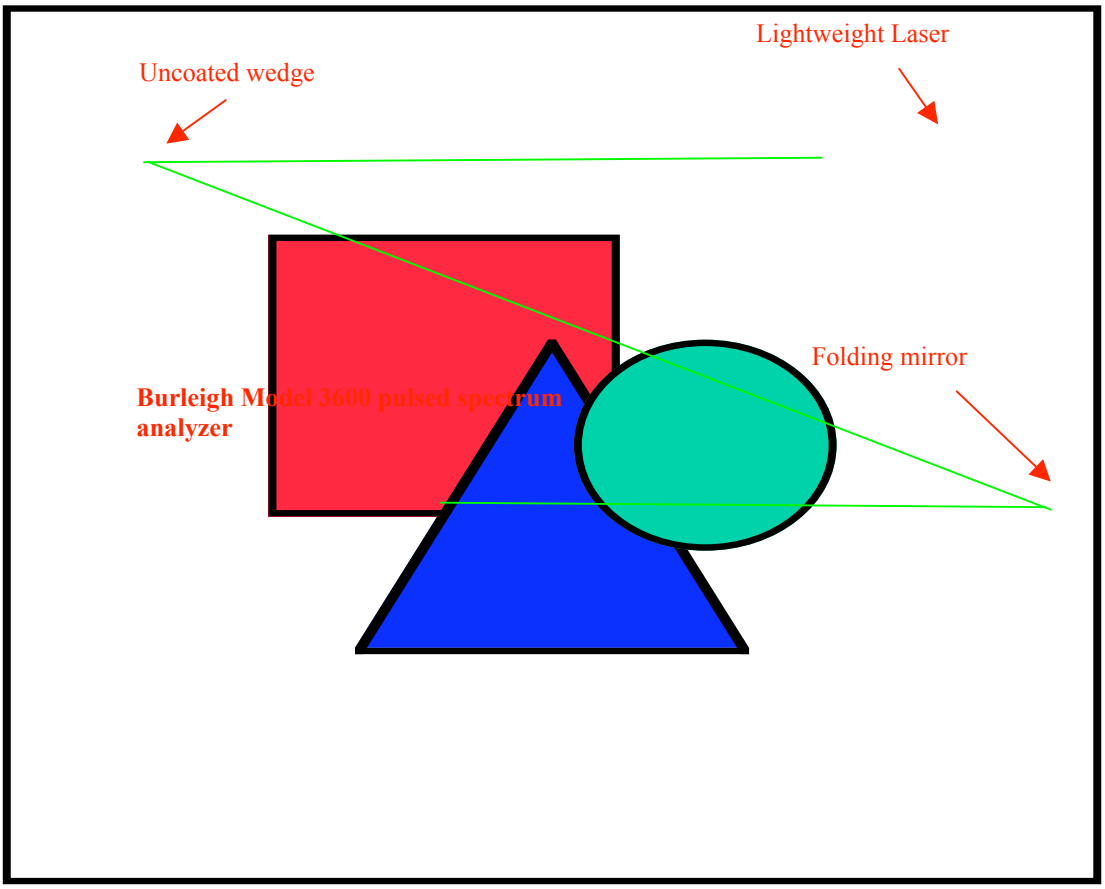

Figure 2. Output spectra for simultaneous 532 nm and 1064 nm operation.

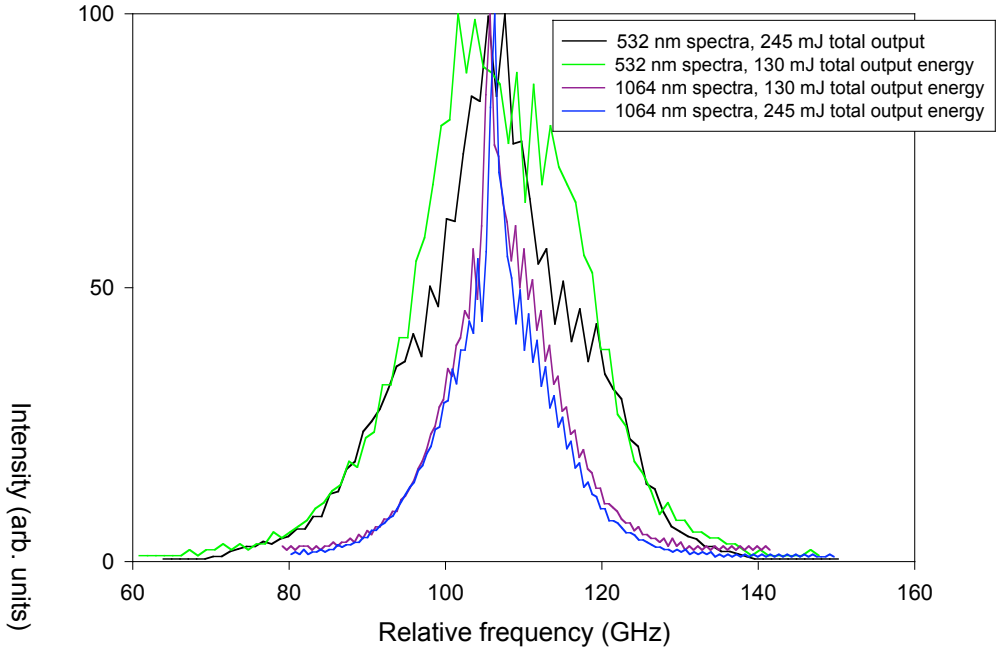

Figure 3. Output spectra for pure 1064 nm operation.

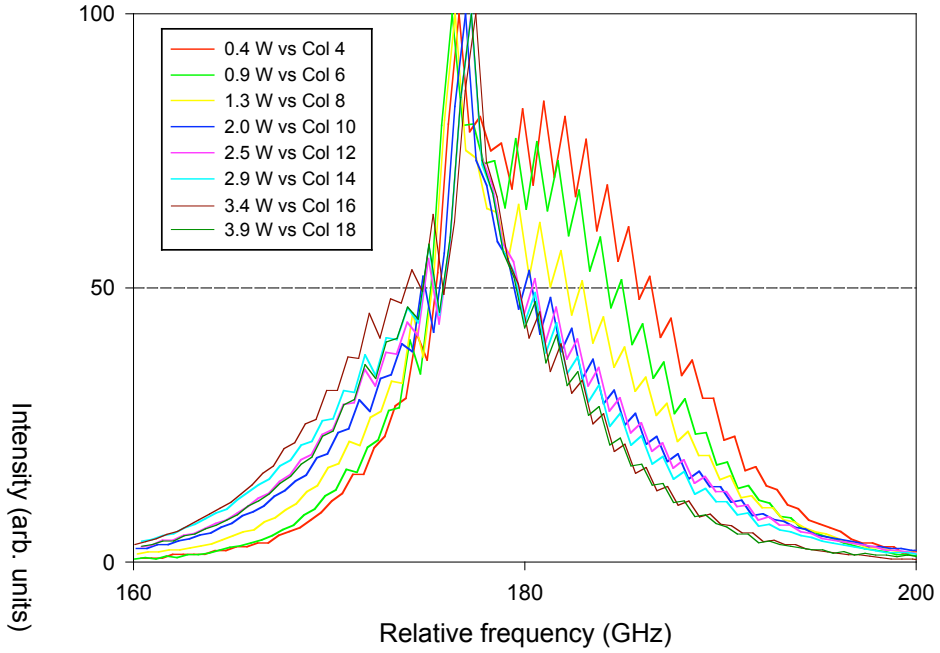

Appendix 1

Summary of Updated RRL Linewidth Measurements

I. Schematic of experimental set-up

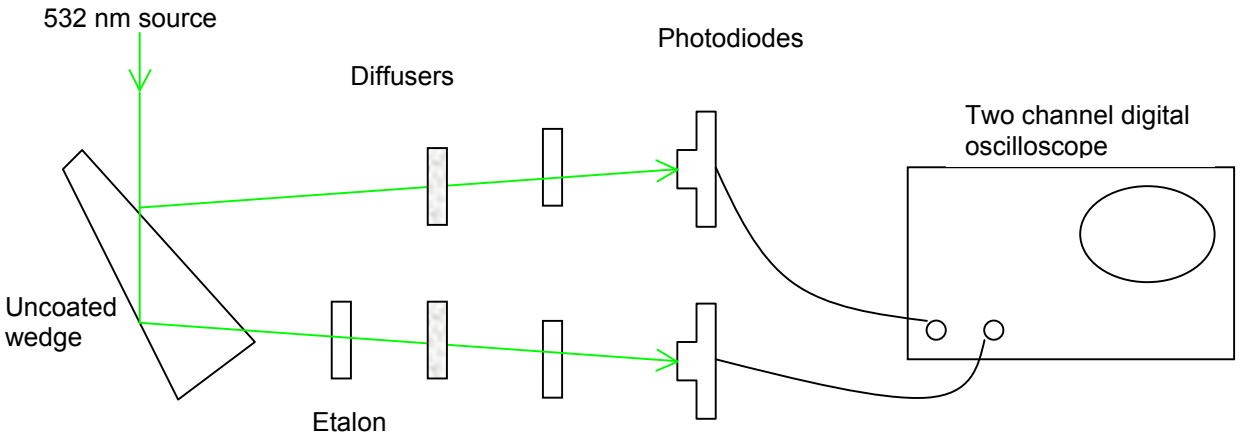

II. 532 nm bandpass filters

A. With the etalon removed, adjust d cilloscope input sensitivities to give equal readings (in screen display units) for the two photodiode input signals.

B. Insert the etalon in one channel. Angle tune the etalon to the first non-normal transmission maximum and optimize the angle for maximum transmitted signal.

C. Record the peak signal from the reference channel (I_o) and the etalon channel (I_{et}). The etalon transmission T is taken as I_{et}/I_o.

III. Results

The results of measurements with 5 different etalons are summarized in Table 1 below. Only etalons which gave visually undistorted transmitted beams at their maximum transmission angles and good extinction between the transmission maxima were used for the data in Table 1. The approach used to calculate the laser linewidth for various line shape functions from the peak transmissions is described in more detail in section IV below.

Table 1. Summary of etalon transmission measurements

Etalon thickness (μm) and #	I_o (arb. units)	I_{et} (abr. units)	T	Flat-topped linewidth* (pm)	Gaussian linewidth* (pm)	Lorentzian linewidth* (pm)
75 μm #1	5.8	3.5	0.60	76	60	29
200 μm #1	5.8	2.7	0.47	42	35	19
300 μm #1	5.8	2.2	0.38	37	31	18
300 μm #2	5.7	2.1	0.37	38	33	19
400 μm #1	5.8	1.6	0.28	41	36	21

*The approach to calculating the laser linewidth is discussed in Section IV.

IV. Overview of linewidth analysis

In order to estimate the laser linewidth from an etalon transmission, it is necessary to assume a lineshape function for spectral distribution of the laser output. The small signal gain of the laser will follow the Lorentzian lineshape of the gain medium fluorescence. Line narrowing of the spectral output occurs because initially the laser output grows as the exponential of the small signal gain, but the exact shape is complicated by gain saturation. This line narrowing effect will result in laser spectral output with reduced content in the wings relative to a Lorentzian distribution. Thus, a fit of the data to a Lorentzian lineshape would be expected to give linewidths that are narrower than the actual linewidths. By similar arguments, a fit of the data to a flat-topped line shape function would be expected to give estimated linewidths that are larger than the actual linewidths. A fit of the data assuming a Gaussian distribution for the spectral output of the laser would give linewidths that are intermediate to the extremes of the Lorentzian and flat-topped distributions. The linewidths from the Gaussian fits are probably the best estimate we can make using this approach. I am open to suggestions as to what might be a better lineshape assumption.

Having assumed a lineshape function for the laser spectral output, the transmission of a given etalon can be calculated from the convolution of the etalon transmission function with the appropriate laser lineshape function. I varied the width of the laser lineshape to find the value that gave a predicted transmission that best agrees with the measured values. Those are the values given in Table 1.

Appendix E

Fibertek High Efficiency 1 Micron Laser Study

Solid-State Pump Laser Efficiency Enhancement.

We have analyzed the performance of the current state-of-the-art diode-pumped lasers, and concluded that there are several areas for efficiency improvement that, when taken together provide a path to obtaining overall electrical efficiencies of 10% in a space-based laser design.

The efficiency of a diode pumped laser can be conveniently divided among serially connected components so that the overall efficiency is the product of the component efficiencies. The improvement in efficiency is then the sum of the percentage efficiency improvements in the individual components. For a diode-pumped solid state laser the system efficiency at one micron can be broken down as:

$$\eta_{sys} = \eta_{pc} * \eta_{diode} * \eta_{pump} * \eta_{extract} \qquad 1)$$

where the component efficiencies are defined as follows:

η_{sys} = overall laser system efficiency
η_{pc} = electrical power conversion efficiency
η_{diode} = diode array electrical efficiency
η_{store} = optical energy storage efficiency
$\eta_{extract}$ = stored energy optical extraction efficiency.

The current state-of-the-art for moderate to high-power diode-pumped lasers is for an overall efficiency of 5 to 6%. For example the NASA/Fibertek VCL prototype transmitter has an electrical efficiency of 6.3%. The VCL transmitter is a small diode-pumped Q-switched slab oscillator operating at an output of 3 W at 240 pps, with passive conductive cooling. An example of a larger system is the diode-pumped laser transmitter built by Fibertek for the Army Long Range Biological Standoff Detection System (LR-BSDS). This system is a diode pumped rod oscillator-amplifier with an output of 100 W at 100 pps. The laser is water-cooled but operates at elevated temperature without active refrigeration. The over-all efficincy of this laser is 5% including power for the heat exchanger. We can use these verified designs as a starting point for projecting technical improvements. Areas of efficiency enhancement are summarized in the following discussion.

- Electrical Power Conversion Efficiency:

The current generation of lasers summarized above uses discreet power converters to generate the pulsed electrical input to the diode arrays. A DC/DC converter is used to convert the power bus to drive voltage for the diode array storage capacitors. A MOSFET-switched modulator then drives the diode arrays with high current (100 A) low duty-cycle (<10%) power. The laser efficiencies sited above were obtained using COTS DC/DC converters that had conversion efficiencies of 80-85%. The MOSFET switched

diode drivers have measured transfer efficiencies of 88%. Therefore the overall efficiency of the electrical power converters was 75%.

Development of an integrated power converter with a design point determined for the specific laser load can raise this efficiency significantly. This has been demonstrated under the NASA VCL flight program where an integrated power converter has been developed by SAIC for NASA Goddard that integrates the DC/DC converter with the diode modulator. Using this approach an overall transfer efficiency of 83% from the DC bus to the diode arrays has been achieved. **This corresponds to a system efficiency improvement of 10% over the conventional approach.** Further improvements in diode driver efficiency have been obtained by Fibertek through the substitution of IGBT switching transistors for MOSFET switches in the diode modulator. The lower series resistance of the IGBTs provides several percent additional improvement in efficiency. The development of dedicated electrical drive circuitry is a low-risk method of achieving significant performance improvement in a diode-pumped space-based laser.

- Diode Array Electrical Efficiency

The diode arrays used in the VCL laser had an electrical efficiency of 45%. This represents the state of the art for long-life 60 W peak-power QCW pump diodes of the type needed for space-based applications. It will be difficult to improve on this performance without compromising lifetime. An incremental improvement can be obtained by reducing the diode heat sink temperature. The coefficient of improvement is approximately 0.3%/°C**. A temperature reduction from 25 C nominal to 15C would therefore produce an approximate 3% improvement in diode electrical efficiency.** This will have to be traded against the implications for the thermal management system.

- Optical Energy Storage Efficiency

The primary area where system efficiency can be realized is in the optical energy storage efficiency of the laser gain medium. This factor includes the optical transfer efficiency between the diode arrays and the laser medium, and the efficiency for storage of the optical energy in the laser gain medium. In a well designed laser pump module such as that used in the VCL or PICASSO prototype program, the transfer efficiency between the diode arrays and the laser materials is near unity. The highest transfer efficiency is obtained in a close-coupled, conductively cooled slab gain module of the type used by Fibertek on both the VCL transmitter and PICASSO prototype. In these modules the diode arrays are optically close-coupled to the gain medium (Nd:YAG) without intervening optics. The transfer efficiency is over 95%. The pump light makes two passes through the slab with an absorption coefficient of 3.2/cm. With a slab thickness of 5-6 mm the absorption efficiency is near 95%. In the particular application considered here, the laser output pulse energy is high and the repetition rate low. In this case it is possible to increase the thickness of the gain media in order to increase the absorption of pump radiation**. By increasing the absorption length from 0.5 to 1 cm we can increase the absorption to over 99%, for an efficiency increase of 4%.**

The storage efficiency is also dependent on the ratio of the pump pulse length to the energy storage time of the medium. Normally the pump pulse length is made as long as possible in order to reduce the number of diode arrays required. For Nd:YAG with a storage lifetime of 240 μs the pump pulse is typically 200 μs. The storage efficiency is given by:

$$\eta = \tau/t\{1-\exp(-t/\tau)\} \qquad 2)$$

where t is the pulse length and τ is the storage time. For a 200 μs pump and 240 μs storage time the efficiency is 67%. This factor can be increased by increasing the storage time or reducing the pump time. Both approaches are amenable to manipulation. Diode manufacturers have recently introduced 100 W peak power QCW diode bars that have comparable efficiency and lifetime as historically used 60 W bars. The additional power can be traded against pulse length, keeping the output energy/bar constant. Thus, the energy output of a 60 W bar pulsed for 200 μs would correspond to a 100 W bar pulsed for 120 μs. For this pulse width, and a 240 μs storage time the storage efficiency rises to 78%. **This provides a 16% system efficiency improvement, with low risk for development.** The cost of the 100 W bars is proportionally higher, but this is not a major driver for a space-based laser.

Another approach to storage efficiency improvement is to utilize a gain medium with a longer storage time. The only material in this category with moderate risk for development is Nd:YLF with a storage lifetime of 480 μs. For the same 200 μs or 120 μs pump pulse widths, the corresponding storage efficiencies are 82% and 88**%. Therefore use of Nd:YLF as a laser material could provide a 22% improvement over Nd:YAG using 200 μs pump, or 13% using 120 μs pump pulses.** The use of Nd:YLF entails some technical risk since this material is not generally available in large sizes required for high power laser. The program would have to bear the cost to support the manufacture of the required material. Nd:YLF also has a higher saturation fluence than Nd:YAG. Therefore, at a particular beam fluence in the laser, the energy extraction efficiency will be lower. The fluence, on the other hand is limited by optical damage in the material. If the damage fluence is comparable in Nd:YLF to that in Nd:YAG, then the extraction efficiency in Nd:YLF will be lower in a pulsed amplifier. This issue requires examination in more detail.

- **Energy Extraction Efficiency**

Energy Extraction depends on the overlap between the pump volume and extracting laser beam and on the fluence of the extracting beam compared to the saturation fluence of the laser material. The maximum energy extraction will be obtained with a flat-topped laser beam. This situation arises from the need to saturate the laser medium uniformly and to reduce ratio of the peak to average fluence in the beam to near unity, in order to avoid optical damage from hot spots in the beam. In the VCL and LR-BSDS lasers discussed above, the beam was either Gaussian or near-Gaussian. The results of our modeling shows that extraction can be improved and optical damage avoided if the laser beam has a super-Gaussian profile of the form.

$$I=I_o\exp(-r/r_o)^n, \qquad 3)$$

where n is the order of the super-Gaussian distribution**. By apodizing the laser beam to produce a super-Gaussian order of 10 or higher, the area overlap between pump and extracting laser beam and the pump distribution can be increased by approximately 20% compared to that for a Gaussian or low-order super-Gaussian.** Apodizing also improves beam propagation by avoiding hard aperture stops that lead to diffractive hot spots in the laser beam. These hot spots can then lead to optical damage.

- **Overall Laser System Efficiency Improvement**

By combining the incremental efficiencies discussed we arrive at a projected overall system efficiency improvement factor of 1.63 for Nd:YAG and 1.70 for Nd:YLF**. Combining these results with the 6% efficiency demonstrated by Fibertek on earlier high-power diode-pumped lasers leads to projected overall efficiencies for optimized space-based diode-pumped lasers of 9 to 10%.** The results of this assessment are summarized in Table 1.

Table 1. Efficiency enhancements possible in diode-pumped solid-state lasers.

Efficiency Enhancement Factor		Nd:YAG	Nd:YLF
Power Conversion		10%	10%
Diode Array		3%	3%
Optical Energy Storage		20%	26%
Optical Extraction		20%	20%
Overall Enhancement		1.64	1.73
Projected Laser System Efficiency		9.8%	10.4%

We also believe that the improvements in beam quality brought about by the apodization of the laser beam discussed above can enhance non-linear steps necessary to convert the laser to the desired UV wavelengths. Since there are at least three nonlinear steps needed to reach the 300-320 nm range from 1.06 μm this enhancement can be significant. The absence of hot spots or diffraction rings also allows the non-linear stages to be driven harder, further increasing the overall efficiency of the laser system. Overall system efficiency enhancements of around 30% over a non-optimized wavelength-converted beam are possible. We recommend that this avenue of investigation be pursued as a high payoff route to laser efficiency enhancement.